

Ruderman-Kittel-Kasuya-Yosida interaction at finite temperature: Graphene and bilayer grapheneN. Klier,¹ S. Shallcross,^{1,*} S. Sharma,² and O. Pankratov¹¹*Lehrstuhl für Theoretische Festkörperphysik, Staudstrasse 7-B2, 91058 Erlangen, Germany*²*Max-Planck-Institut für Mikrostrukturphysik Weinberg 2, D-06120 Halle, Germany*

(Received 31 December 2014; published 12 November 2015)

We investigate the Ruderman-Kittel-Kasuya-Yosida (RKKY) interaction between magnetic impurities in both single layer and Bernal stacked bilayer graphene, finding a number of striking anomalies in the temperature dependence of this interaction. In undoped single layer graphene the strength of the RKKY interaction for substitutional impurities anomalously increases upon increasing temperature, an effect that persists up to and beyond room temperature. For impurities *intercalated* in the Bernal stacked bilayer and a doping that places the chemical potential near the antibonding band edge, a *qualitative change of the RKKY interaction with temperature* occurs: a low-temperature oscillatory interaction develops into a high-temperature antiferromagnetic coupling, accompanied by an overall increase of the interaction strength. The origin of the temperature anomalies can be traced back to specific features of the density of states: the vanishing density of states at the apex of the Dirac cone in single layer graphene, and the “kink” in the density of states at the antibonding band edge in the case of the Bernal bilayer.

DOI: [10.1103/PhysRevB.92.205414](https://doi.org/10.1103/PhysRevB.92.205414)

PACS number(s): 73.20.At, 73.21.Ac

I. INTRODUCTION

The indirect exchange interaction between magnetic impurities, known as the Ruderman-Kittel-Kasuya-Yosida (RKKY) interaction, is governed by the static spin susceptibility of the host system and therefore depends sensitively on the host electronic structure. For this reason the RKKY interaction is particularly interesting for materials in which the underlying electronic spectrum is novel. It is for this reason that the research on low dimensional carbon systems, initiated by the discovery of graphene in 2004 [1], has been accompanied by an interest in the RKKY interaction in such systems.

In the case of graphene, a two-dimensional honeycomb lattice of carbon, the electronic spectrum at low energies consists of conical manifolds situated at the high-symmetry K and K' points that occur at the vertices of the hexagonal Brillouin zone [1–3]. This spectrum, along with the bipartite lattice structure where the two sublattices give rise to a pseudospin space, the additional electronic degree of freedom, leads to a situation in which the low-energy excitations are described by the Dirac-Weyl equation [4,5] of massless neutrinos. This novel electronic spectrum leads, at $T = 0$, to a monotonic RKKY with a R^{-3} decay envelope for undoped graphene [6–8] for which the Fermi energy is coincident with the Dirac point. For doped graphene [9], on the other hand, the oscillatory R^{-2} RKKY characteristic of a normal two-dimensional metal is found.

The RKKY interaction in graphene is further removed from that of a normal metal by the presence of the inequivalent K and K' points in the Brillouin zone. Scattering between the Dirac cones situated at these points leads to a factor in the propagator that oscillates *on the scale of graphene's lattice constant* [6–10]. Realistic magnetic impurities in any graphene

based system must have an atomic radius substantially greater than the nearest-neighbor distance of graphene ($a_{nn} = 1.42 \text{ \AA}$), and therefore the exchange field of each impurity will couple to multiple carbon atoms. In combination with a propagator that oscillates on the scale of a_{nn} , this leads to an unusual situation in which the asymptotic form of the magnetic interaction is sensitive to the local structure of the graphene-impurity complex. For example, at the Dirac point of graphene a R^{-7} decay is found for the plaquette impurity geometry [11], in contrast to the R^{-3} decay for substitutional impurities. Note that in this work we use the notation substitutional impurity to refer to a *contact interaction* between an impurity spin and the Dirac gas [9].

While the $T = 0$ RKKY interaction in monolayer graphene is now well understood, the RKKY interaction continues to be a subject of intense research in more complex graphene-type systems with investigations of RKKY at the edges of finite graphene samples [7,10,12,13], the role of disorder in the RKKY interaction [14,15], and the RKKY in AB stacked bilayer graphene [11,16–18]. A remarkable transition in the RKKY interaction as a function of doping occurs in the latter system that is asymptotically discontinuous: for Fermi energies just below the antibonding band edge there is an oscillatory interaction with a wavelength of $\lambda = 15a$ (a is the lattice constant of graphene), while just above the antibonding band edge the interaction becomes antiferromagnetic.

A natural question to ask is how the RKKY in these systems is manifest at finite temperatures. Surprisingly, despite it being much more relevant experimentally, the RKKY at finite temperature has not received the same attention as the zero-temperature case. In a normal metal the RKKY interaction is slightly damped at increasing temperatures as the Fermi surface becomes smeared out. However, in single layer graphene the vanishing number of states at the Dirac point in combination with a linear excitation spectrum (in contrast to the parabolic excitation spectrum of the Schrödinger gas) suggests that this smearing could be outweighed by the increase in the number of states available for scattering. Indeed,

*phsss@tfkp.physik.uni-erlangen.de

for the conductivity of graphene on SiC it has been shown that the vanishing density of states at the Dirac point leads to an anomalous temperature dependence of the resistance (which decreases with increasing temperature due to the additional states that become available for transport) [19,20]. On the other hand, the profoundly rapid change in the form of the RKKY interaction as a function of Fermi energy near the antibonding band edge of the AB bilayer spectrum suggests that finite temperature smearing out this energy region may lead to a highly nontrivial temperature dependence for this system. It is the purpose of the present paper to investigate the finite temperature behavior of the RKKY in monolayer and bilayer graphene, and establish the precise nature of such anomalous behavior. For both of these systems the following question also arises: Given the sensitivity of the $T = 0$ magnetic interaction to local impurity environment, will the temperature dependence of the RKKY be similarly sensitive to the impurity-graphene geometry?

For substitutional impurities in undoped single layer graphene we find that the strength of the RKKY interaction *increases with increasing temperature*, an effect that, remarkably, persists up to (and beyond) room temperature for $R < 20a$ (a is the lattice constant of graphene). On the other hand for doped single layer graphene the behavior of a normal metal is recovered: a finite temperature damping of the $T = 0$ interaction. For the more realistic plaquette type of impurity we find that the qualitative form of the temperature dependence is *determined by the nature of the coupling of the plaquette impurities to the Dirac gas*. For the “incoherent” coupling scheme that includes only on-site spin flips we recover a normal temperature dependence, i.e., the RKKY interaction monotonically decreases in magnitude with increasing temperature for both doped and undoped graphene. In contrast, whereas for several of the “coherent” coupling schemes that include intersite spin flips the temperature dependence shows again an anomalous increase in magnitude with increasing temperature.

In the case of the RKKY interaction in the Bernal bilayer we focus on the intercalated impurities as these appear most likely to be realized experimentally [21,22]. We find that discontinuities in the asymptotics of the RKKY interaction found at $T = 0$ are rapidly smoothed with increasing temperature, such that at room temperature no trace of these zero-temperature singularities can be detected. However, the most striking result is that for the intercalated impurity we find an RKKY interaction whose *qualitative form changes with temperature*: a low-temperature oscillatory interaction develops into a high-temperature antiferromagnetic interaction. This behavior can be understood as a consequence of the temperature smearing which averages over the very distinct RKKY behaviors that occur at $T = 0$ in a narrow energy range at the antibonding band edge.

The remainder of the paper is structured as follows. In Sec. II we present the basic theory that underpins our treatment of the indirect exchange interaction and introduce the notational conventions that we follow. In Secs. III and IV we present the finite temperature RKKY interaction for single and bilayer graphene respectively, and Sec. V concludes the paper.

II. BASIC THEORY AND NOTATION

In this section we briefly summarize the notations and formalism that will be used throughout this paper in order to describe the finite temperature RKKY interaction. Our general approach will be to derive exactly the real-space finite temperature Green’s function, which is possible for both single layer and AB stacked bilayer graphene, and then use standard finite temperature perturbation theory for the Hamiltonian $H = H^0 - \lambda H'$, where H^0 is the single or bilayer Hamiltonian and H' the perturbation due to the spin impurities. The size disparity between a realistic magnetic impurity and the graphene lattice will, in general, result in a situation in which each impurity couples to *several* carbon atoms, and the formalism must take account of this.

To this end, we first consider two impurities \mathbf{S}_1 and \mathbf{S}_2 that couple to a set of surrounding carbon atoms M_1 and M_2 . In our model we assume that impurity \mathbf{S}_1 causes a scattering of the Dirac electrons from site $a_2 \in M_1$ with spin ν to site $a_1 \in M_1$ with spin μ . Similarly \mathbf{S}_2 is responsible for scattering of Dirac electrons between sites that surround the second impurity and are part of the set M_2 , i.e., scattering from a site $a_3 \in M_2$ with spin ν to site $a_4 \in M_2$ with spin μ . The interaction Hamiltonian H' is then obtained as a sum of all these scattering processes each weighted with an individual coupling constant $\lambda(a_{2i-1}, a_{2i})$, i.e.,

$$H' = -\frac{\hbar}{2} \sum_{i=1}^2 \sum_{\mu, \nu} \sum_{a_{2i-1}, a_{2i} \in M_i} \lambda(a_{2i-1}, a_{2i}) c_{a_{2i-1}\mu}^\dagger c_{a_{2i}\nu} (\boldsymbol{\sigma}_{\mu\nu} \cdot \mathbf{S}_i), \quad (1)$$

where $\boldsymbol{\sigma}$ is the vector of Pauli matrices and the operator $c_{a_{2i-1}\mu}^\dagger (c_{a_{2i}\nu})$ creates (annihilates) an electron at site a_{2i-1} (a_{2i}) with spin μ (ν). We briefly comment on a key feature of this model which is that while the environment information of the impurity spin in the form of coupling to several carbon atoms is retained, the electronic form of the coupling at each of these atoms is a contact interaction. Going beyond this approximation would entail a detailed first-principles study of the local hybridization between the magnetic impurity and the surrounding carbon atoms. In the present study all such physics essentially goes into the contact coupling constant $\lambda(a_{2i-1}, a_{2i})$. We go beyond previous studies that use this model [6,8,9] by allowing the coupling constants $\lambda(a_{2i-1}, a_{2i})$ to be different at each site, but including the full nonlocality of the impurity-Dirac gas interaction must be reserved for a further first-principles study. The utility of this model arises from the multivalley nature of graphene, which leads to a term in the propagator that oscillates fast on the scale of the lattice constant. This, in turn, implies that the local geometry of the impurity will be crucial for the RKKY interaction due to interference effects arising from the multiple-scattering paths between the carbon atoms of each impurity environment, a situation quite different from, e.g., the propagator in a noble-metal host such as Cu, which does not contain such a “fast oscillation” part. The impact of this local geometry and of the consequent interference effects is precisely what is captured by this model.

Derived in the usual way the resulting RKKY interaction of two impurities is given as $E^{\text{RKKY}} = (\mathbf{S}_1 \cdot \mathbf{S}_2) \mathcal{J}^{\text{coh}}$, with the

exchange integral taking on the somewhat complex form

$$\begin{aligned} \mathcal{J}^{\text{coh}} &= \frac{1}{2\beta} \sum_{a_1, a_2 \in M_1} \sum_{a_3, a_4 \in M_2} \lambda(a_1, a_2) \lambda(a_3, a_4) \\ &\times \sum_n \mathcal{G}_{\alpha(a_4)l(a_4)\alpha(a_1)l(a_1)}^0(\mathbf{r}_{a_4} - \mathbf{r}_{a_1}, i\omega_n) \\ &\times \mathcal{G}_{\alpha(a_2)l(a_2)\alpha(a_3)l(a_3)}^0(\mathbf{r}_{a_2} - \mathbf{r}_{a_3}, i\omega_n). \end{aligned} \quad (2)$$

In this expression $\mathbf{r}_{a_1}, \mathbf{r}_{a_2} (\mathbf{r}_{a_3}, \mathbf{r}_{a_4})$ are the position vectors of the carbon atoms in the cluster $M_1 (M_2)$. The finite temperature Green's function $\mathcal{G}_{\alpha(a_4)l(a_4)\alpha(a_1)l(a_1)}^0(\mathbf{r}_{a_4} - \mathbf{r}_{a_1}, i\omega_n)$ is a function of the separation vector $\mathbf{r}_{a_4} - \mathbf{r}_{a_1}$ and the Matsubara frequency $\omega_n = (2n + 1)\pi/(\hbar\beta)$ with $\beta = 1/(k_B T)$ and where k_B stands for the Boltzmann constant. The subscript indices of \mathcal{G}^0 indicate, e.g., that the vector \mathbf{r}_{a_1} refers to the site on sublattice $\alpha(a_1)$ of layer $l(a_1)$, and similarly for all other such indices.

The possibility of intersite spin flips at each impurity implies the possibility of a four-site contribution to the RKKY interaction. It should be stressed, however, that this is *not* a higher-order process in terms of the Green's function of the host Dirac gas, which would result in a non-Heisenberg coupling ($\mathbf{S}_1 \cdot \mathbf{S}_2$)².

As a special case of this formalism we have the situation of substitutional impurities (where it is reasonable to consider a single-site exchange coupling only) for which the Hamiltonian reads

$$H' = -\frac{\hbar\lambda}{2} \sum_{i=1}^2 \sum_{\mu, \nu} c_{i\mu}^\dagger c_{i\nu} (\boldsymbol{\sigma}_{\mu\nu} \cdot \mathbf{S}_i) \quad (3)$$

and the interaction energy between the two impurities is now conveniently written as

$$E_{\alpha_i \alpha'_i}^{\text{RKKY}}(\mathbf{R}) = (\mathbf{S}_1 \cdot \mathbf{S}_2) \mathcal{J}_{\alpha_i \alpha'_i}(\mathbf{R}) \quad (4)$$

with the exchange integral given by the usual form,

$$\mathcal{J}_{\alpha_i \alpha'_i}(\mathbf{R}) = \frac{\lambda^2}{2\beta} \sum_n \mathcal{G}_{\alpha_i \alpha'_i}^0(-\mathbf{R}, i\omega_n) \mathcal{G}_{\alpha'_i \alpha_i}^0(\mathbf{R}, i\omega_n), \quad (5)$$

where in this expression $\mathcal{G}^0(\mathbf{R}, i\omega_n)$ is now given as a function of the distance vector $\mathbf{R} = \mathbf{r}_2 - \mathbf{r}_1$. In polar coordinates the distance vector takes the form (R, θ) with $\theta = \arctan y/x$. The sublattice of the impurity at position \mathbf{r}_1 is indicated by $\alpha \in \{A, B\}$ and the layer of the impurity by $l \in \{1, 2\}$. In order to specify the sublattice and the layer of the second impurity we use the indices α' and l' .

III. SINGLE LAYER GRAPHENE

Our strategy here will be to first calculate the real-space finite-temperature Green's function for single layer graphene, from which we may derive immediately the RKKY interaction

TABLE I. Coefficients for the low-energy expansion at each of the six high-symmetry K points of the graphene Brillouin zone.

m	1	2	3	4	5	6
$\mathbf{K} \times \frac{3a}{2\pi}$	$\begin{pmatrix} 2 \\ 0 \end{pmatrix}$	$\begin{pmatrix} -2 \\ 0 \end{pmatrix}$	$\begin{pmatrix} 1 \\ \sqrt{3} \end{pmatrix}$	$\begin{pmatrix} -1 \\ \sqrt{3} \end{pmatrix}$	$\begin{pmatrix} 1 \\ -\sqrt{3} \end{pmatrix}$	$\begin{pmatrix} -1 \\ -\sqrt{3} \end{pmatrix}$
γ	0	π	$-\frac{\pi}{3}$	$\frac{2\pi}{3}$	$\frac{\pi}{3}$	$-\frac{2\pi}{3}$
δ	-1	+1	+1	-1	+1	-1

for substitutional impurities via Eq. (5). We subsequently consider the asymptotic RKKY for large impurity separations, for which compact analytical expressions may easily be obtained. Numerical results are then presented for substitutional impurities for both the exact and asymptotic versions of the RKKY, as well as the more realistic plaquette impurity.

A. Finite temperature RKKY interaction in single layer graphene: Theory

In order to construct the RKKY at finite temperatures we evidently require the finite temperature real-space Green's function for single layer graphene. To this end we consider the graphene Hamiltonian $H_m^0(\mathbf{k})$ in a low-energy expansion close to the m th corner of the hexagonal Brillouin zone. For simplicity we consider a model that takes only nearest-neighbor hopping into account. By inversion we find the finite temperature \mathbf{k} -space Green's function of single layer graphene $\mathcal{G}_m^0(\mathbf{k}, i\omega_n) = \hbar [i\hbar\omega_n + \mu - H_m^0(\mathbf{k})]^{-1}$,

$$\begin{aligned} \mathcal{G}_m^0(\mathbf{k}, i\omega_n) &= \frac{\hbar}{(i\hbar\omega_n + \mu)^2 - |\tilde{\Phi}_m(\mathbf{k})|^2} \\ &\times \begin{pmatrix} i\hbar\omega_n + \mu & \tilde{\Phi}_m(\mathbf{k}) \\ \tilde{\Phi}_m^*(\mathbf{k}) & i\hbar\omega_n + \mu \end{pmatrix}, \end{aligned} \quad (6)$$

where μ stands for the chemical potential and where we have defined the function $\tilde{\Phi}_m(\mathbf{k}) = \hbar v_F k e^{i(\gamma_m + \delta_m \phi_{\mathbf{k}})}$. In this expression the reciprocal space vector \mathbf{k} represents a small deviation from the corner \mathbf{K}_m and is in polar coordinates given by $(k, \phi_{\mathbf{k}})$ with $\phi_{\mathbf{k}} = \tan^{-1} k_y/k_x$. Furthermore, the Fermi velocity is given by $v_F = \sqrt{3}at/(2\hbar)$ where t is the nearest neighbor hopping amplitude and a graphene's lattice constant. The two phases γ_m and δ_m are tabulated in Table I; see also Ref. [11].

The corresponding real-space Green's function is obtained in the usual low-energy approximation,

$$\mathcal{G}^0(\mathbf{R}, i\omega_n) = \frac{1}{3} \sum_{m=1}^6 \mathcal{G}_m^0(\mathbf{R}, i\omega_n) e^{i\mathbf{K}_m \cdot \mathbf{R}}, \quad (7)$$

with $\mathcal{G}_m^0(\mathbf{R}, i\omega_n) = 1/\Omega_{BZ} \int d^2k \exp(i\mathbf{k} \cdot \mathbf{R}) G_m^0(\mathbf{k}, i\omega_n)$ and the area of the Brillouin zone given by $\Omega_{BZ} = 8\pi^2/(\sqrt{3}a^2)$. The sum in Eq. (7) is taken over all six K points and can be reduced to a sum over the two inequivalent ones. A Fourier transform of Eq. (6) then yields the real-space Green's function as

$$\mathcal{G}_m^0(\mathbf{R}, i\omega_n) = -\frac{2\pi i(\hbar\omega_n - i\mu)}{\hbar v_F^2 \Omega_{BZ}} \mathcal{M}(\mathbf{R}, i\omega_n) \quad (8)$$

with the matrix $\mathcal{M}(\mathbf{R}, i\omega_n)$ given by

$$\mathcal{M}(\mathbf{R}, i\omega_n) = \begin{pmatrix} K_0(\text{sgn}(\omega_n) \frac{\hbar\omega_n - i\mu}{\hbar v_F} R) & \text{sgn}(\omega_n) \Phi_m(\mathbf{R}) K_1(\text{sgn}(\omega_n) \frac{\hbar\omega_n - i\mu}{\hbar v_F} R) \\ \text{sgn}(\omega_n) \Phi_m^*(\mathbf{R}) K_1(\text{sgn}(\omega_n) \frac{\hbar\omega_n - i\mu}{\hbar v_F} R) & K_0(\text{sgn}(\omega_n) \frac{\hbar\omega_n - i\mu}{\hbar v_F} R) \end{pmatrix} \quad (9)$$

and where we have introduced the function $\Phi_m(\mathbf{R}) = e^{i(\gamma_m + \delta_m \theta)}$. In these expressions $K_\nu(x)$ represents the modified Bessel function of the second kind and ν th order, and to obtain this result we have used the standard integrals $\int_0^\infty d\varphi \exp[ikR \cos(\varphi - \theta)] = 2\pi J_0(kR)$ and $\int_0^\infty dk [kJ_0(kR)]/(k^2 + z^2) = K_0(zR)$ [note that the last integral requires the real part of z to be positive valued which accounts for the appearance of $\text{sgn}(\omega_n)$ in the above result].

From the real-space Green's function Eq. (8) and the expression for the RKKY interaction, Eq. (5), we immediately find the interaction for the situation in which both impurities are on the same sublattice (AA) is given by

$$\mathcal{J}_{AA}(\mathbf{R}) = \frac{16}{\pi\beta} C f_{AA}(\mathbf{R}) \sum_{n=-\infty}^{+\infty} \left(\frac{\hbar\omega_n - i\mu}{\hbar v_F} \right)^2 \times K_0 \left(\text{sgn}(\omega_n) \frac{\hbar\omega_n - i\mu}{\hbar v_F} R \right)^2, \quad (10)$$

while for the case in which the impurities couple to different sublattices (BA) we similarly find

$$\mathcal{J}_{BA}(\mathbf{R}) = -\frac{16}{\pi\beta} C f_{BA}(\mathbf{R}) \sum_{n=-\infty}^{+\infty} \left(\frac{\hbar\omega_n - i\mu}{\hbar v_F} \right)^2 \times K_1 \left(\text{sgn}(\omega_n) \frac{\hbar\omega_n - i\mu}{\hbar v_F} R \right)^2. \quad (11)$$

Here we have introduced for notational convenience the constant $C = -\lambda^2 \hbar^2 a^2 / (64\pi t^2)$. In both these expressions the sum over the $6 \times 6 = 36$ different combinations of special K points has been taken. It should be emphasized that there are of course only two inequivalent cones, and the sum of 36 combinations rather than $2 \times 2 = 4$ combinations of special K points is purely a matter of convenience. The result of this sum is a prefactor to the RKKY expression from intervalley scattering (i.e., scattering between inequivalent Dirac cones), the so-called fast oscillation functions $f_{\alpha\alpha'}(\mathbf{R})$. These temperature-independent functions are identical to the equivalent functions found in the $T = 0$ RKKY interaction [8,9] and are given by

$$f_{AA}(\mathbf{R}) = 1 + \cos[\mathbf{K}_2 \cdot \mathbf{R}], \quad (12)$$

$$f_{BA}(\mathbf{R}) = 1 + \cos[\mathbf{K}_2 \cdot \mathbf{R} + \pi - 2\theta]. \quad (13)$$

It is curious that while the intravalley scattering is temperature dependent, the intervalley scattering is temperature independent. That the $T = 0$ results for the RKKY interaction in single layer graphene are recovered in the $T \rightarrow 0$ limit of Eqs. (10) and (11) may be seen via the usual route in which

the Matsubara sum goes over, as $T \rightarrow 0$, to an integral

$$\frac{1}{\hbar\beta} \sum_{n=-\infty}^{+\infty} \rightarrow \frac{1}{2\pi} \int_{-\infty}^{+\infty} d\omega. \quad (14)$$

For undoped monolayer graphene the resulting zero-temperature integrals can be taken analytically,

$$\mathcal{J}_{AA}(\mathbf{R}) = \frac{\hbar v_F}{2R^3} C f_{AA}(\mathbf{R}), \quad (15)$$

$$\mathcal{J}_{BA}(\mathbf{R}) = -\frac{3\hbar v_F}{2R^3} C f_{BA}(\mathbf{R}), \quad (16)$$

where we have used $\int_{-\infty}^{\infty} dx x^2 K_0(|x|)^2 = \pi^2/16$ and $\int_{-\infty}^{\infty} dx x^2 K_1(|x|)^2 = 3\pi^2/16$. These are the well-known results for the RKKY interaction in undoped graphene at $T = 0$ [8]. To show that for doped graphene the results (10) and (11) limit to their $T = 0$ counterparts is not possible directly. However this can be proven easily for the asymptotic in R versions of Eqs. (10) and (11), as we will now show. (Note that we take the asymptotic limit $Rk_F \gg 0$ but that as the doping is finite this is equivalent to an asymptotic expansion in R .)

The required asymptotic forms of the RKKY interaction may be obtained by the replacement in Eqs. (10) and (11) of the modified Bessel functions by the appropriate large distance asymptotics. For brevity of presentation we consider explicitly only the case in which the impurities reside on the same sublattice, Eq. (10). This equation goes over asymptotically to

$$\mathcal{J}_{AA}(\mathbf{R}) = \frac{8}{\beta R} C f_{AA}(\mathbf{R}) \sum_{n=-\infty}^{+\infty} \left[\text{sgn}(\omega_n) \frac{\hbar\omega_n - i\mu}{\hbar v_F} - \frac{1}{4R} \right] \times e^{-2R \text{sgn}(\omega_n) (\hbar\omega_n - i\mu) / (\hbar v_F)}, \quad (17)$$

from which we can notice that the Matsubara sum may straightforwardly be evaluated by the introduction of a derivative with respect to R :

$$\mathcal{J}_{AA}(\mathbf{R}) = -\frac{4C f_{AA}(\mathbf{R})}{R} \left(\frac{d}{dR} + \frac{1}{2R} \right) k_B T \times \sum_{n=-\infty}^{+\infty} e^{-2R \text{sgn}(\omega_n) (\hbar\omega_n - i\mu) / (\hbar v_F)}. \quad (18)$$

The Matsubara sum is now a geometric series and upon insertion of $\omega_n = (2n + 1)\pi / (\hbar\beta)$ into Eq. (18) we find

$$k_B T \sum_{n=-\infty}^{+\infty} e^{-2R \text{sgn}(\omega_n) (\hbar\omega_n - i\mu) / (\hbar v_F)} = \cos \left(\frac{2\mu}{\hbar v_F} R \right) F_1, \quad (19)$$

where we have defined

$$F_1 = \frac{k_B T}{\sinh \left(\frac{2\pi k_B T R}{\hbar v_F} \right)}. \quad (20)$$

Substitution of this result into Eq. (18) finally leads to

$$\mathcal{J}_{AA}(\mathbf{R}) = \frac{8Cf_{AA}(\mathbf{R})}{\hbar v_F R} F_1 \left[\mu \sin\left(\frac{2\mu}{\hbar v_F} R\right) + \pi F_2 \cos\left(\frac{2\mu}{\hbar v_F} R\right) - \frac{\hbar v_F}{4R} \cos\left(\frac{2\mu}{\hbar v_F} R\right) \right], \quad (21)$$

in which we have further defined

$$F_2 = \frac{k_B T}{\tanh\left(\frac{2\pi k_B T R}{\hbar v_F}\right)} \quad (22)$$

that results from taking the R derivative of F_1 . For the case of impurities on different sublattices an entirely analogous calculation yields

$$\mathcal{J}_{BA}(\mathbf{R}) = -\frac{8Cf_{BA}(\mathbf{R})}{\hbar v_F R} F_1 \left[\mu \sin\left(\frac{2\mu}{\hbar v_F} R\right) + \pi F_2 \cos\left(\frac{2\mu}{\hbar v_F} R\right) + \frac{3\hbar v_F}{4R} \cos\left(\frac{2\mu}{\hbar v_F} R\right) \right]. \quad (23)$$

In order to confirm that the result known from the $T = 0$ RKKY analysis of single layer graphene emerges from the finite temperature analysis presented above, we expand Eqs. (21) and (23) about $T = 0$ up to second order in T . For \mathcal{J}_{AA} given by Eq. (21) this procedure then yields

$$\mathcal{J}_{AA}(\mathbf{R}) = \frac{4}{\pi R^2} C f_{AA}(\mathbf{R}) \left\{ \mu \sin\left(\frac{2\mu}{\hbar v_F} R\right) + \frac{\hbar v_F}{4R} \times \cos\left(\frac{2\mu}{\hbar v_F} R\right) - \frac{2\pi^2 k_B^2 R^2}{3\hbar^2 v_F^2} T^2 \left[\mu \sin\left(\frac{2\mu}{\hbar v_F} R\right) - \frac{3\hbar v_F}{4R} \cos\left(\frac{2\mu}{\hbar v_F} R\right) \right] \right\} \quad (24)$$

while similarly for \mathcal{J}_{BA} we find

$$\mathcal{J}_{BA}(\mathbf{R}) = -\frac{4}{\pi R^2} C f_{BA}(\mathbf{R}) \left\{ \mu \sin\left(\frac{2\mu}{\hbar v_F} R\right) + \frac{5\hbar v_F}{4R} \times \cos\left(\frac{2\mu}{\hbar v_F} R\right) - \frac{2\pi^2 k_B^2 R^2}{3\hbar^2 v_F^2} T^2 \left[\mu \sin\left(\frac{2\mu}{\hbar v_F} R\right) + \frac{\hbar v_F}{4R} \cos\left(\frac{2\mu}{\hbar v_F} R\right) \right] \right\}. \quad (25)$$

Reassuringly, we see that the zeroth-order term in each of these results is precisely that of the RKKY result found via zero-temperature formalism [9]. Note that the $T \rightarrow 0$ and $\mu \rightarrow 0$ limit of Eqs. (24) and (25) may not be taken at the same time, and thus we cannot recover Eqs. (15) and (16). This follows from the fact that Eqs. (24) and (25) are both obtained from the large argument asymptotic form of the Bessel function in Eqs. (10) and (11) and, evidently, when both $T \rightarrow 0$ and $\mu \rightarrow 0$ this asymptotic form is no longer valid. This is a finite temperature manifestation of a similar situation at $T = 0$ in which the $\mu \rightarrow 0$ and $\mathbf{R} \rightarrow \infty$ limits cannot be interchanged (see, e.g., Refs. [8,9]), and that setting $\mu = 0$ in the long-distance asymptotics of the RKKY interaction at finite doping does not recover the corresponding asymptotic RKKY result of undoped graphene.

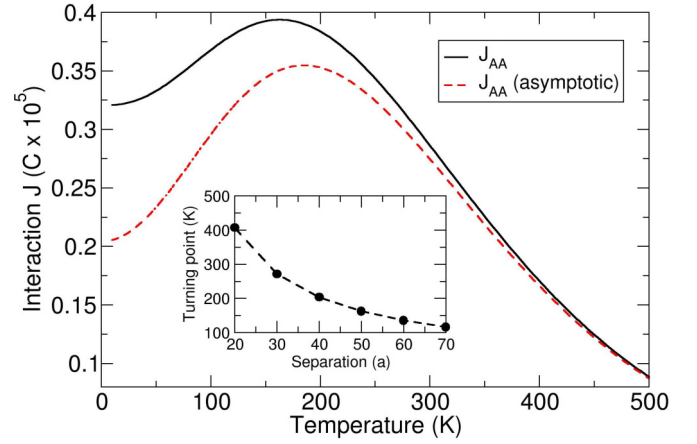


FIG. 1. (Color online) Temperature dependence of the impurity interaction for two spin moments on the A sublattice of pristine graphene ($\mu = 0$ eV). The full (black) line is the exact RKKY result of Eq. (10) while the broken (red) line is the asymptotic result, valid for large R , given by Eq. (21). The interaction \mathcal{J} is measured in terms of the coupling constant C and multiplied by a factor of 10^5 ; positive values correspond to ferromagnetic coupling and negative to antiferromagnetic coupling. The impurities are separated by $50a$ (with a the graphene lattice constant), and the impurity vector is taken to be in the armchair direction. Other possible sublattice combinations yield similar results. The inset displays the turning point in the temperature dependence as a function of the separation.

B. Finite temperature RKKY interaction in single layer graphene: Numerical results

We now consider the numerical evaluation of the exact RKKY given by Eqs. (10) and (11), and in particular the comparison of these exact RKKY formulas with the asymptotic forms derived in the previous section.

We first consider the temperature dependence of the functions $F_{1,2}$. It is interesting to note that for large T the function F_2 increases linearly in T while the function F_1 decreases exponentially for large T ; evidently the function $F_1 F_2$ is nonmonotonic and there must exist a turning point in $F_1 F_2$ at some finite T . On this basis we might expect a *nonmonotonic temperature dependence* of the RKKY interaction in single layer graphene, and this indeed proves to be the case for undoped graphene. Shown in Fig. 1 is the RKKY interaction for impurities on the same sublattice, Eq. (10), for undoped graphene as a function of temperature at a fixed impurity separation of $50a$. Shown also is the corresponding asymptotic result given by Eq. (21), which is seen to be in good agreement, in particular for the high-temperature regime.

Strikingly, the strength of the interaction increases as a function of T , with a turning point at a temperature of 153 K. As we have discussed in the introduction, an RKKY interaction that increases in magnitude with temperature is to be expected for undoped graphene as the increase in the states available for scattering countervails, for low enough temperatures, the exponential damping introduced by the smearing of the Fermi surface at finite temperatures. The inset of Fig. 1 displays the turning point in temperature, i.e., that temperature above which the magnitude of the RKKY interaction decreases with increasing temperature. Interestingly, the larger R is the *smaller*

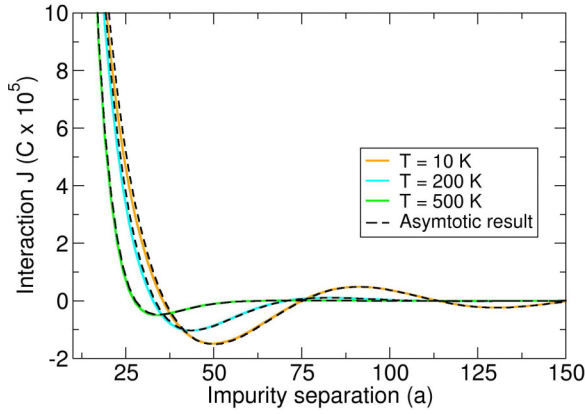


FIG. 2. (Color online) Shown is the RKKY interaction for A sublattice impurities in doped graphene ($\mu = 0.1$ eV) as a function of impurity separation and for temperatures $T = 10$ K, $T = 200$ K, and $T = 500$ K. In all cases the impurity separation vector is in the armchair direction. The asymptotic result [see Eq. (21)] is also shown as the broken line. The interaction \mathcal{J} is measured in terms of the coupling constant C and multiplied by a factor 10^5 ; positive values correspond to ferromagnetic coupling and negative to antiferromagnetic coupling.

the temperature region in which the anomalous behavior is seen. Indeed, it may be seen that for $R < 20a$ the anomalous temperature effect persists up to room temperature and, for smaller impurity separations, far beyond room temperature. This behavior may be understood, in a qualitative way, by noting that while increasing T leads to an increasing energy range contributing to the interaction, increasing R counteracts this by driving the energy range back to the Fermi surface as, following the usual stationary phase argument, the higher frequency oscillations lead to cancellation of contributions except at the border of the energy range, i.e., at the Fermi energy.

Turning to doped single layer graphene, one might expect that for sufficiently large chemical potential μ the first term of Eqs. (21) and (23) would dominate the nonmonotonic $F_1 F_2$ factor associated with the second term. As may be seen from Fig. 2 this occurs already at $\mu = 0.1$ eV. Shown in this figure is the RKKY interaction for impurities on the same sublattice, Eq. (10), as a function of separation and for a range of temperatures. As can clearly be seen the physics of the finite temperature RKKY for doped graphene is simply that of the usual exponential damping observed in normal metals. Additionally, we show the asymptotic form of \mathcal{J}_{AA} , for which the agreement with the exact RKKY is seen to be very good in all cases.

We now turn to the RKKY interaction for complex impurity geometries. This is motivated by the size disparity that any realistic magnetic atom, e.g., a lanthanide or transition-metal atom, will have with the graphene lattice. As the atomic radius of these metal atoms is comparable to the nearest-neighbor distance of graphene, the situation of substitutional impurities is rendered somewhat unrealistic. This case, however, provides a basis for understanding more complex and realistic situations. We now consider the plaquette impurity in which the magnetic atom is positioned at the center of the honeycomb of the

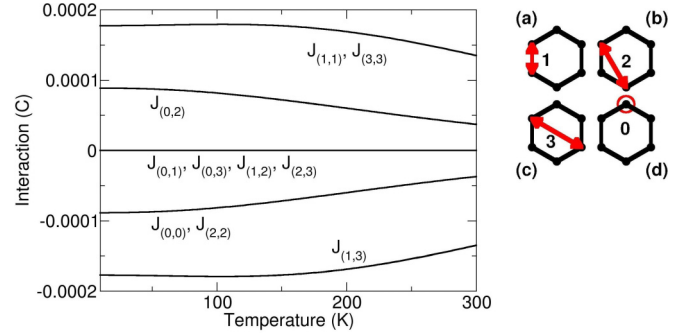


FIG. 3. (Color online) Temperature dependence of RKKY interaction for plaquette impurities separated by $R = 20a$ (with a the lattice constant of graphene). The interaction \mathcal{J} is measured in terms of the coupling constant C ; positive values correspond to ferromagnetic coupling and negative to antiferromagnetic coupling. In each case the nature of the coupling of the plaquette impurity to the graphene layer is indicated by the label $\mathcal{J}_{(i,j)}$: this represents the RKKY interaction between two plaquette impurities in which the first (second) impurity couples via spin flips between i th (j th) nearest-neighbor carbon atoms or via on-site spin flips $i, j = 0$. These processes are illustrated in the right-hand panel of the figure for spin flips between (a) first, (b) second, (c) third nearest neighbors, and (d) on-site spin flips. Evidently, the nature of the *local coupling* has a pronounced effect on the temperature dependence.

graphene lattice. This impurity will couple to all six carbon atoms of the honeycomb and, in the absence of a realistic (i.e., first principles) calculation, we must make some assumptions concerning this coupling. In particular, one may have both *on site* spin flip processes as well as *intersite* spin flip processes between any two of the carbon atoms on this hexagon. We adopt a pragmatic approach and consider just two distinct ways in which the plaquette impurity couples to the Dirac gas: (i) via on-site spin flips, and (ii) via spin flips between n th nearest-neighbor carbon atoms.

As may be seen from Fig. 3 the plaquette geometry results in just three distinct nearest-neighbor vectors on the carbon honeycomb; see (a)–(c) of the right hand panel. There are then just 4×4 possibilities for the interaction of two impurities, of which ten are distinct. For notational convenience we label each of these interactions by $\mathcal{J}_{(i,j)}$ in which i, j represent the type of coupling which may consist of on-site spin flips ($i, j = 0$) or n th nearest-neighbor spin flips ($i, j = n$). For each of these cases the temperature dependence is shown in Fig. 3, where the impurity separation is fixed to $20a$. The impact of the form of the impurity coupling is strikingly evident from this figure: both the form of the temperature dependence as well as the sign of the interaction are determined by the local coupling rather than the intrinsic properties of the Dirac gas. One may observe that there are two distinct types of low-temperature behavior, a monotonic decrease in the magnitude of the interaction shown by $\mathcal{J}_{(0,0)}$, $\mathcal{J}_{(0,2)}$, and $\mathcal{J}_{(2,2)}$ as well as a nonmonotonic behavior exhibited by $\mathcal{J}_{(1,1)}$, $\mathcal{J}_{(1,3)}$, and $\mathcal{J}_{(3,3)}$. All other cases result in a complete cancellation of the interaction.

It is worth reflecting on this somewhat unusual situation in which the *local coupling* of the impurities to the Dirac gas affects profoundly the *asymptotic interaction* between such

impurities. At the heart of this is the fact that the propagator of the Dirac gas contains a part, due to the multivalley nature of the graphene spectrum, that oscillates on the scale of the lattice constant. This renders the RKKY interaction in graphene highly sensitive to the details of the local coupling in contrast to the “classical” RKKY interaction, for instance, of Fe in fcc Cu, which is not.

IV. BERNAL STACKED BILAYER GRAPHENE

We now turn to the temperature dependence of the RKKY interaction in AB stacked bilayer graphene. The AB bilayer is interesting from the point of view of experimentally realizing the RKKY in graphene for two reasons: (i) the well-known intercalation of graphite suggests it may be possible to dilutely intercalate the bilayer with magnetic impurities, and (ii) the impurity confinement between the two graphene layers may lead to a strong coupling with the Dirac gas, a requirement for a realistic manifestation of the RKKY. Experiments exist in which bilayer graphene has been intercalated with metals from the first group of the Periodic Table such as Li and Rb [21,22] and, furthermore, the intercalation of graphite by impurity atoms has been successfully studied many times experimentally in the past. These experimental findings indicate that the intercalation of the bilayer by magnetic impurities should be possible, however to the best of our knowledge there does not yet exist an experiment in which magnetic atoms have been intercalated into bilayer graphene.

The intercalated impurity resides at the most open position of the bilayer, which occurs when the impurity center lies on the line connecting the center of a graphene honeycomb in the first layer and the nonbonding carbon atom in the second layer. In a recent paper Klier *et al.* uncovered an unusually rich $T = 0$ structure of the RKKY as a function of Fermi energy near the antibonding band edge in the AB bilayer for this impurity geometry [11]. Whether this part of the bilayer spectrum may be accessed experimentally remains a moot point. However, the significant shifting of the Fermi level entailed by, e.g., depositing graphene on a SiC (0001) face, and the subsequent shifting of the Fermi level back to the Dirac point with doping by a complex organic electron acceptor [23], gives rise to the hope that a judicious combination of substrate and doping effects may render the antibonding band-edge region of the spectrum accessible to experiment.

Given that at finite temperature energies in a range $k_B T$ contribute to the RKKY interaction, an unusual $T = 0$ behavior as a function of Fermi energy might be expected to lead to a correspondingly unusual finite temperature behavior. We will therefore focus on the temperature dependence of the RKKY for the intercalated impurity in the AB bilayer, and to that end briefly review the main result of Ref. [11].

In the left-hand panel of Fig. 4 is shown the band structure of the bilayer with the antibonding band edge indicated by the broken light-shaded (red) line. The antibonding band edge separates two distinct regions in which for $\mu < E_g$ one has a single Fermi circle, while for $\mu \geq E_g$ there exist two distinct Fermi circles: one from the low-energy chiral band manifold as well one from the high-energy antibonding manifold. As the asymptotic RKKY interaction is driven by the spanning

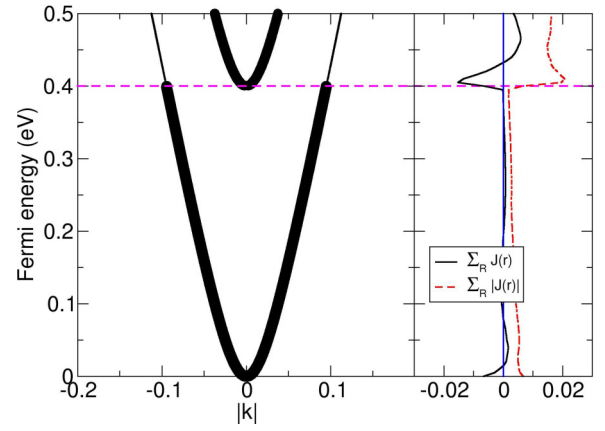


FIG. 4. (Color online) Left-hand panel: band structure of the AB bilayer in which the width of the band line represents the contribution of that band to the asymptotic RKKY interaction between intercalated impurities in the bilayer. Evidently, the antibonding band edge is associated with a *switching* of the Fermi surface that drives the interaction from the low-energy chiral band to the high-energy antibonding band. The right-hand panel illustrates the impact this has on the RKKY interaction via the quantities $\sum_{R>R_c} J(\mathbf{R})$ and $\sum_{R>R_c} |J(\mathbf{R})|$. The former will, by cancellation, be close to zero for an oscillatory interaction and attain its maximum value for a monotonic interaction while the latter quantity measures the strength of the RKKY interaction. Clearly, as the Fermi energy crosses the antibonding band edge the “switching” of the Fermi circle driving the RKKY interaction results in a rapid change of the RKKY both in form and in magnitude.

vectors of the Fermi surface it may thus be written as

$$J(\mathbf{R}) = \frac{2C}{\pi R^2} [W^+ \sin 2k_F^+ R + W^- \sin 2k_F^- R + (-1)^{l-l'} W^{+-} \sin(k_F^+ + k_F^-) R], \quad (26)$$

i.e., as a weight function multiplying the oscillatory function governed by each of the three possible Fermi-surface spanning vectors from two Fermi circles: $2k_F^+$ (the spanning vector of the “outer” low-energy chiral Fermi surface), $2k_F^-$ (the spanning vector of the “inner” high-energy Fermi surface), and $(k_F^+ + k_F^-)$ (a spanning vector between these two Fermi surfaces). The width of the band line in the left-hand panel of Fig. 4 is weighted by the contribution of that band to the RKKY using these weight functions: the low-energy band manifold contributes a weight $W^+ + W^{+-}/2$ to the asymptotic RKKY interaction, and high-energy band manifold contributes a weight $W^- + W^{+-}/2$ (the weight from inter-Fermi-surface scattering W^{+-} we simply share equally between the low- and high-energy manifolds). At each energy the weights are normalized such that they sum to unity. As may be seen from Fig. 4, when the Fermi energy crosses the antibonding band edge—indicated by the broken line—a remarkable “switching off” of the low-energy Fermi surface occurs. Just below the antibonding band edge the RKKY is governed by the only spanning vector that exists, that of the chiral band $k_F^+ = \sqrt{2}t_{\perp}/(\hbar v_F)$. However, just above the antibonding band edge the contribution of this low-energy chiral band to the RKKY is negligible as compared to that from the high-energy antibonding band, for which near the antibonding band edge we have $k_F^- \approx 0$.

This switching off of one spanning vector at the antibonding band edge, and the switching on of a different one, leads to a *discontinuous change in the asymptotic RKKY interaction* that limits to $\lambda = \pi/k_F^+ = \pi\hbar v_F/(\sqrt{2}t_\perp)$ as $E_F \rightarrow E_g$ from below the antibonding band edge, while it limits to $\lambda = \pi/k_F^- \rightarrow \infty$ from above the antibonding band edge. The physics behind this remarkable switching off of the low-energy Fermi surface at the antibonding band edge has been investigated in detail in Ref. [11], and the underlying mechanism has been identified as arising from interference effects between the multiple RKKY scattering paths between the carbon atoms within the coupling environment of each magnetic impurity. This effect is seen most strongly for intercalated impurities in the incoherent approximation, but is also seen in many (but not all) coherent RKKY sums; see again Ref. [11].

In order to describe the changing RKKY interaction at the antibonding band edge, it is useful to introduce a pair of numbers which characterize *globally* the interaction with regard to (i) its oscillatory or monotonic [antiferromagnetic (AFM)] character and (ii) its overall strength. To that end we present in the right-hand panel of Fig. 4 the quantities $\sum_{R>R_c} J(\mathbf{R})$ and $\sum_{R>R_c} |J(\mathbf{R})|$ as a function of Fermi energy. The former of these quantities will be close to zero for an oscillatory interaction, but will assume its maximum value for the case of a monotonic interaction, while the second is simply a measure of the overall strength of the interaction. In each sum there is a lower cutoff of $R_c = 10a$ which we introduce in order to exclude the preasymptotic regime from the summation. As may be seen from Fig. 4 there is a step change at the antibonding band edge in both these quantities indicating (i) a change from oscillatory to monotonic behavior has occurred along with (ii) a significant increase in the strength of the RKKY for $E > E_g$.

In order to determine how this rich antibonding band-edge structure influences the finite temperature RKKY interaction for this system we follow the strategy deployed in the previous section for single layer graphene: we first determine an exact analytical form for the finite temperature Green's function of the host *AB* bilayer, and subsequently use this to derive the RKKY interaction via the formalism of Sec. II.

A. Finite temperature RKKY in the *AB* bilayer: Theory

We proceed in an analogous fashion to the case of single layer graphene by first inverting the standard low-energy bilayer Hamiltonian $H_m^0(\mathbf{k})$ at the m th corner of the Brillouin zone to yield the \mathbf{k} -space finite temperature Green's function $\mathcal{G}_m^0(\mathbf{k}, i\omega_n) = \hbar[i\hbar\omega_n + \mu - H_m^0(\mathbf{k})]^{-1}$. The corresponding real-space Green's function is obtained by a Fourier transform as

$$\mathcal{G}^0(\mathbf{R}, i\omega_n) = \frac{1}{3} \sum_{m=1}^6 \mathcal{G}_m^0(\mathbf{R}, i\omega_n) e^{i\mathbf{K}_m \cdot \mathbf{R}} \quad (27)$$

and we thus require the Fourier transform of $\mathcal{G}_m^0(\mathbf{k}, i\omega_n)$ which yields

$$\mathcal{G}_m^0(\mathbf{R}, i\omega_n) = -\frac{i\pi}{\hbar v_F^2 \Omega_{BZ}} \mathcal{M}(\mathbf{R}, i\omega_n),$$

where for simplicity of presentation we have defined the matrix $\mathcal{M}(\mathbf{R}, i\omega_n)$ in Table II.

TABLE II. Real-space Green's function of *AB*-stacked bilayer graphene $\mathcal{G}_{m,\alpha_i\alpha'_j}^0(\mathbf{R}, i\omega_n) = -i\pi/(\hbar v_F^2 \Omega_{BZ}) \mathcal{M}_{\alpha_i\alpha'_j}(\mathbf{R}, i\omega_n)$. Each matrix element $\mathcal{M}_{\alpha_i\alpha'_j}(\mathbf{R}, i\omega_n)$ is represented by a linear combination of modified Bessel functions $K_\nu(x)$. The argument of each Bessel function is given by $z^+ R = \sqrt{(\hbar\omega_n - i\mu)(\hbar\omega_n - i\mu - it_\perp)} R / (\hbar v_F)$ or $z^- R = \sqrt{(\hbar\omega_n - i\mu)(\hbar\omega_n - i\mu + it_\perp)} R / (\hbar v_F)$. The square root must be taken so that the real part of z^+ and z^- is positive valued.

$\alpha_i\alpha'_j$	$\mathcal{M}_{\alpha_i\alpha'_j}(\mathbf{R}, i\omega_n)$
A_1A_1	$(\hbar\omega_n - i\mu)[K_0(z^+R) + K_0(z^-R)]$
A_1B_1	$\hbar v_F \Phi_m^*(\mathbf{R})[z^+K_1(z^+R) + z^-K_1(z^-R)]$
A_1A_2	$(\hbar\omega_n - i\mu)[K_0(z^+R) - K_0(z^-R)]$
A_1B_2	$\hbar v_F \Phi_m(\mathbf{R})[z^+K_1(z^+R) - z^-K_1(z^-R)]$
B_1A_1	$\hbar v_F \Phi_m(\mathbf{R})[z^+K_1(z^+R) + z^-K_1(z^-R)]$
B_1B_1	$(\hbar\omega_n - i\mu - it_\perp)K_0(z^+R) + (\hbar\omega_n - i\mu + it_\perp)K_0(z^-R)$
B_1A_2	$\hbar v_F \Phi_m(\mathbf{R})[z^+K_1(z^+R) - z^-K_1(z^-R)]$
B_1B_2	$\frac{\hbar^2 v_F^2}{\hbar\omega_n - i\mu} \Phi_m^2(\mathbf{R})[z^{+2}K_2(z^+R) - z^{-2}K_2(z^-R)]$
A_2A_1	$(\hbar\omega_n - i\mu)[K_0(z^+R) - K_0(z^-R)]$
A_2B_1	$\hbar v_F \Phi_m^*(\mathbf{R})[z^+K_1(z^+R) - z^-K_1(z^-R)]$
A_2A_2	$(\hbar\omega_n - i\mu)[K_0(z^+R) + K_0(z^-R)]$
A_2B_2	$\hbar v_F \Phi_m(\mathbf{R})[z^+K_1(z^+R) + z^-K_1(z^-R)]$
B_2A_1	$\hbar v_F \Phi_m^*(\mathbf{R})[z^+K_1(z^+R) - z^-K_1(z^-R)]$
B_2B_1	$\frac{\hbar^2 v_F^2}{\hbar\omega_n - i\mu} \Phi_m^{*2}(\mathbf{R})[z^{+2}K_2(z^+R) - z^{-2}K_2(z^-R)]$
B_2A_2	$\hbar v_F \Phi_m^*(\mathbf{R})[z^+K_1(z^+R) + z^-K_1(z^-R)]$
B_2B_2	$(\hbar\omega_n - i\mu - it_\perp)K_0(z^+R) + (\hbar\omega_n - i\mu + it_\perp)K_0(z^-R)$

We will consider explicitly here the case in which the intercalated impurity couples to the bilayer gas via on-site spin flips, and thus the relevant result of Sec. II for calculating the RKKY is Eq. (5). Following the same formal route as taken in the case of the single layer, the results of Table II may be directly inserted into Eq. (5) and the sum over the K points taken (i.e., a sum over m) to yield the RKKY interaction for the bilayer.

Similarly to the single layer case, we find that the exchange integral factorizes into the product of an intravalley and an intervalley term,

$$\mathcal{J}_{\alpha_i\alpha'_j}(\mathbf{R}) = C \mathcal{I}_{\alpha_i\alpha'_j}(R) f_{\alpha_i\alpha'_j}(\mathbf{R}), \quad (28)$$

with $C = -\frac{\lambda^2 \hbar^2 a^2}{64\pi I^2}$, $\mathcal{I}_{\alpha_i\alpha'_j}(R)$ the intravalley term that describes the response of the Dirac gas, and $f_{\alpha_i\alpha'_j}(\mathbf{R})$ an intervalley factor that encodes the scattering between the two inequivalent Dirac cones. In principle, there are 16 of these functions in the bilayer case. However, as has been detailed in Ref. [11], there are only six inequivalent $\mathcal{J}_{\alpha_i\alpha'_j}(\mathbf{R})$ due to the symmetry of the bilayer. Furthermore, there are only three distinct fast oscillation terms, of which two have been presented in Eqs. (12) and (13),

$$f_{A_1A_1}(\mathbf{R}) = f_{AA}(\mathbf{R}), \quad (29)$$

$$f_{B_1A_1}(\mathbf{R}) = f_{BA}(\mathbf{R}), \quad (30)$$

$$f_{B_2B_1}(\mathbf{R}) = 1 + \cos[\mathbf{K}_2 \cdot \mathbf{R} + 4\theta]. \quad (31)$$

TABLE III. The finite temperature RKKY interaction in Bernal stacked bilayer graphene. The exchange integral is expressed as $\mathcal{J}_{\alpha_l\alpha'_l}(\mathbf{R}) = C f_{\alpha_l\alpha'_l}(\mathbf{R}) \mathcal{I}_{\alpha_l\alpha'_l}(R)$ in which $\mathcal{I}_{\alpha_l\alpha'_l}(R)$ is the *intravalley* contribution that describes the response of the Dirac gas, and $f_{\alpha_l\alpha'_l}(\mathbf{R})$ an *intervalley* term that encodes scattering between the two inequivalent Dirac cones. The coefficient C is given by $C = -\lambda^2 \hbar^2 a^2 / (64\pi t^2)$ where λ is the coupling strength, a is the lattice constant of graphene, and t is the amplitude of the nearest-neighbor hopping for graphene. The table defines the function $\mathcal{I}_{\alpha_l\alpha'_l}(R)$; the factor $f_{\alpha_l\alpha'_l}(\mathbf{R})$ may be read off from Eqs. (29)–(31).

$\alpha_l\alpha'_l$	$\mathcal{I}_{\alpha_l\alpha'_l}(R)$	$f_{\alpha_l\alpha'_l}(\mathbf{R})$
A_1A_1	$\frac{4}{\pi\beta} \sum_n \left(\frac{\hbar\omega_n - i\mu}{\hbar v_F}\right)^2 [K_0(z^+R) + K_0(z^-R)]^2$	$f_{A_1A_1}(\mathbf{R})$
A_2A_1	$\frac{4}{\pi\beta} \sum_n \left(\frac{\hbar\omega_n - i\mu}{\hbar v_F}\right)^2 [K_0(z^+R) - K_0(z^-R)]^2$	$f_{A_1A_1}(\mathbf{R})$
B_1B_1	$\frac{4}{\pi\beta} \sum_n \left(\frac{\hbar v_F}{\hbar\omega_n - i\mu}\right)^2 [z^{+2}K_0(z^+R) + z^{-2}K_0(z^-R)]^2$	$f_{A_1A_1}(\mathbf{R})$
B_2B_1	$\frac{4}{\pi\beta} \sum_n \left(\frac{\hbar v_F}{\hbar\omega_n - i\mu}\right)^2 [z^{+2}K_2(z^+R) - z^{-2}K_2(z^-R)]^2$	$f_{B_2B_1}(\mathbf{R})$
B_1A_1	$-\frac{4}{\pi\beta} \sum_n [z^+K_1(z^+R) + z^-K_1(z^-R)]^2$	$f_{B_1A_1}(\mathbf{R})$
B_2A_1	$-\frac{4}{\pi\beta} \sum_n [z^+K_1(z^+R) - z^-K_1(z^-R)]^2$	$f_{B_1A_1}(-\mathbf{R})$

The expressions for the finite temperature RKKY are somewhat cumbersome, and we present them in Table III.

Following the approach for single layer graphene described in Sec. III we might attempt to analytically evaluate the Matsubara sums of the finite temperature RKKY by means of introducing an asymptotic approximation for the hyperbolic Bessel functions. In the case of the bilayer we found this attempt was ultimately frustrated by the square-root function present in both z^+ and z^- ; see Table II. We therefore proceed by numerically evaluating the Matsubara sums of the expressions in Table III.

B. Finite temperature RKKY in the AB bilayer: Numerical results

We now consider the numerical evaluation of the finite temperature RKKY interaction for the intercalated impurity. As we consider only on-site spin flips this is given by a simple linear combination of the substitutional impurity forms presented in Table III. There are ten carbon atoms that couple to each impurity: six from the honeycomb of one layer and four from the other layer (the nonbonding carbon atom and its three nearest neighbors). This leads to a sum over $10 \times 10 = 100$ substitution forms which after simplification [11] yields the result

$$\begin{aligned}
 \mathcal{J}^{\text{int}}(\mathbf{R}) = & 9C [2\mathcal{I}_{A_1A_1}(R) + 2\mathcal{I}_{A_2A_1}(R) \\
 & + \mathcal{I}_{B_1B_1}(R) + 2\mathcal{I}_{B_2A_1}(R) + 2\mathcal{I}_{B_1A_1}(R)] \\
 & + 6C \left(\frac{\lambda_2}{\lambda_1}\right) [\mathcal{I}_{B_2B_1}(R) + \mathcal{I}_{B_1A_1}(R) + \mathcal{I}_{B_2A_1}(R)] \\
 & + C \left(\frac{\lambda_2}{\lambda_1}\right)^2 \mathcal{I}_{B_1B_1}(R) f_{A_1A_1}(\mathbf{R}), \quad (32)
 \end{aligned}$$

where $\mathcal{I}_{\alpha_l\alpha'_l}$ may be read off from Table III.

In Fig. 5 we present the RKKY interaction plotted as a function of impurity separation for several doping levels. The rapid change of the RKKY at the antibonding band edge can be

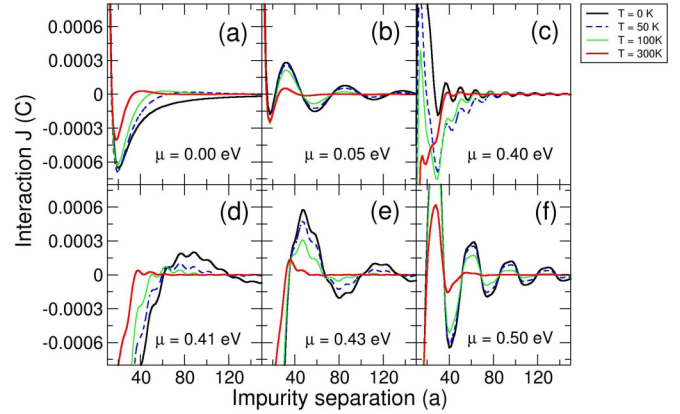


FIG. 5. (Color online) Anomalous temperature behavior at the antibonding band edge: The RKKY interaction for intercalated impurities shown as a function of separation for six different doping levels of the bilayer, and in each case for the temperatures 10, 100, 200, and 300 K. The interaction \mathcal{J} is measured in terms of the coupling constant C ; positive values corresponding to ferromagnetic coupling and negative to antiferromagnetic coupling. In all panels the impurity separation vector is taken in the armchair direction. At doping levels that place the chemical potential far from the antibonding band edge ($E_g = 0.4$ eV) the RKKY interaction shows the expected temperature damping, i.e., the form of the interaction is preserved while the amplitude decreases with increasing temperature. However, at the antibonding band edge (c), a strikingly different temperature dependence may be observed in that (i) the form of the RKKY interaction itself changes with temperature, from a low-temperature oscillatory behavior to a high-temperature antiferromagnetic behavior, and (ii) the magnitude of the interaction increases with temperature.

seen in the period of the RKKY oscillation, which is markedly different for $\mu = 0.40$ eV [panel (c)] and $\mu = 0.41$ eV [panel (d)]. As has been mentioned in the opening of this section, this is a manifestation of a switching of the spanning vector driving the RKKY interaction from the large momentum Fermi circle of the chiral band to the small momentum Fermi circle of the antibonding band.

We now consider the temperature dependence of the RKKY interaction for each of these doping levels. With the exception of panel (c), for which the doping level places the chemical potential at the antibonding band edge, one observes the behavior of a normal metal; the form of the $T = 0$ RKKY interaction is preserved while the amplitude of the oscillation continuously reduces with increasing T . In contrast, the temperature dependence exhibited at the antibonding band edge is qualitatively different: an increase in temperature from 0 to 50 K results in a change in form of the RKKY interaction from oscillatory to antiferromagnetic.

The change in the form of the RKKY interaction with the doping level at $T = 0$ is therefore mirrored in a corresponding change of the RKKY interaction with temperature. This is, needless to say, quite different from the temperature-induced damping of the RKKY that occurs at other doping levels and indeed is seen in the standard manifestation of the RKKY between magnetic impurities in nonmagnetic metal hosts, for instance in fcc Cu.

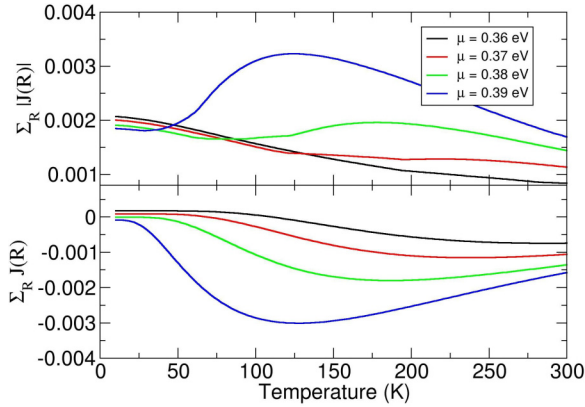


FIG. 6. (Color online) Temperature dependence of the sums $\sum_{R>R_c} \mathcal{J}(\mathbf{R})$ (lower panel) and $\sum_{R>R_c} |\mathcal{J}(\mathbf{R})|$ as a function of temperature for chemical potentials of 0.36, 0.37, 0.38, and 0.39 eV. The first of these two sums will be close to zero in the case of an oscillatory interaction, and attain its largest value and be equal in magnitude to the second sum for a monotonic interaction. This second sum evidently simply measures the strength of the RKKY interaction. As may be seen in the lower panel of this figure, there is a crossover from a low-temperature oscillatory form to a monotonic (AFM) form of the interaction with increasing temperature. At this crossover the magnitude of the interaction also increases significantly (see upper panel). For chemical potentials placed further from the antibonding band edge this crossover occurs at higher temperatures, before being lost altogether.

Two natural questions now suggest themselves: (i) how close to the antibonding band edge does the chemical potential need to be placed to observe the temperature anomaly, and (ii) how does the temperature at which the oscillatory to AFM transition occurs depend on the position of the chemical potential? As the chemical potential is moved further below the antibonding band edge, higher temperatures will be required to access the AFM region above the anti-bonding band edge. On these grounds one anticipates that the oscillatory form of the RKKY will persist to higher temperatures for doping levels that place the chemical potential further below from the antibonding band edge.

To answer these questions it is useful to plot the quantities $\sum_{R>R_c} \mathcal{J}(\mathbf{R})$ and $\sum_{R>R_c} |\mathcal{J}(\mathbf{R})|$ as a function of temperature for chemical potentials near the antibonding band edge. In Fig. 6 both these quantities are displayed for chemical potentials from $E_g - 0.01$ eV to $E_g - 0.04$ eV. For the case of $E_g - 0.01$ one may note that the quantity $\sum_{R>R_c} \mathcal{J}(\mathbf{R})$, plotted in the lower panel of Fig. 6, remains close to zero only for a very small temperature range of ≈ 10 K before assuming a pronounced negative value, indicating that for this doping the oscillatory behavior is seen only at very low temperatures $T < 10$ K. The corresponding plot of $\sum_{R>R_c} |\mathcal{J}(\mathbf{R})|$ in the upper panel of Fig. 6 shows a distinct increase in magnitude for the temperature at which the oscillatory to AFM transition in $\mathcal{J}(\mathbf{R})$ occurs, indicating a sharp increase in strength of the interaction. This can be understood from the fact that above the antibonding band edge the $T = 0$ interaction not only changes from oscillatory to AFM but, as may be seen in Fig. 4, also increases markedly in magnitude. As the transition from

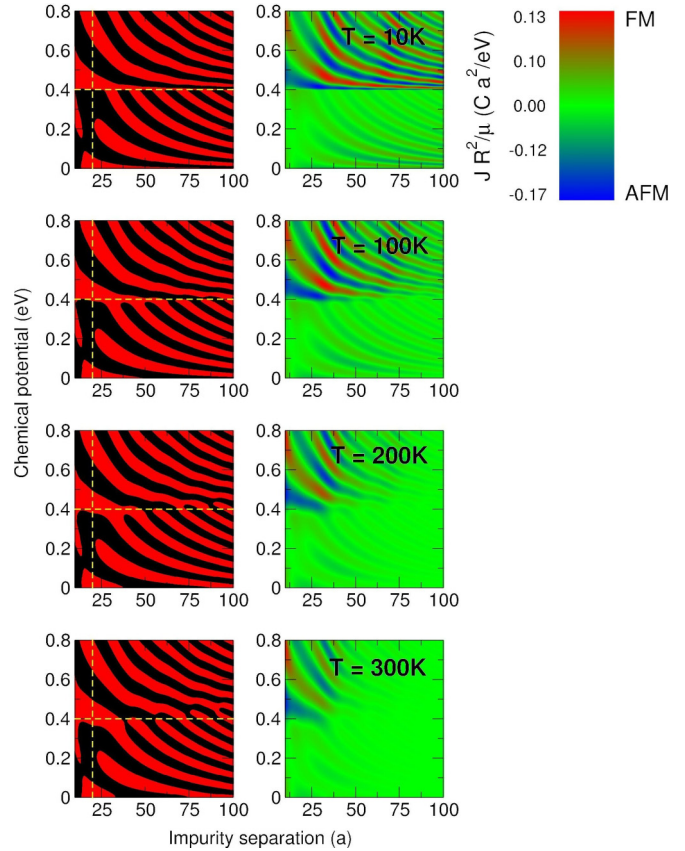


FIG. 7. (Color online) Overview of the temperature-dependent RKKY interaction for the intercalated impurity geometry. The right-hand column shows the RKKY interaction (scaled by R^2/μ for clarity), while the left-hand column displays the regions of ferromagnetic and antiferromagnetic interaction, indicated by the dark (black) shaded and light shaded (red) areas respectively. While the $T = 0$ discontinuity at 0.4 eV in the interaction may still be observed at 10 K, it is progressively smoothed out with increasing temperature as the FM and AFM bands merge across the $T = 0$ discontinuity. The vertical lines are at $R = 20a$ and the interaction on these lines is displayed in Fig. 8; the horizontal lines indicate the gap energy of $E_g = 0.4$ eV.

oscillatory to AFM is induced by temperature smearing into the RKKY interaction energies from above the antibonding band edge, such smearing will evidently result in an increase in strength of the interaction as seen in Fig. 6.

We now consider the question of how the position of the chemical potential changes the temperature at which the transition in the interaction occurs. As may be seen from the plots for $\mu = E_g - n$ eV with $n = 0.02$, $n = 0.03$, and $n = 0.04$, placing the chemical potential further from the antibonding band edge results, as expected, in the $T = 0$ oscillatory interaction persisting to increasingly higher temperatures. Eventually, for $\mu < E_g - 0.03$ eV the energy region above the gap cannot be accessed by Fermi smearing and no transition is observed.

We finally present an overview of the RKKY interaction for the intercalated impurity as a function of impurity separation and chemical potential for a series of temperatures $T = 10$ K, $T = 100$ K, $T = 200$ K, and $T = 300$ K; see Fig. 7. In

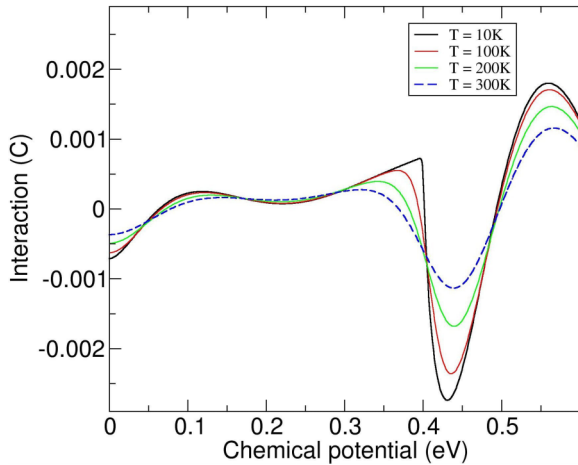


FIG. 8. (Color online) Temperature smearing of the RKKY antibonding band-edge singularity: Shown is the RKKY interaction as a function of doping for intercalated magnetic impurities for temperatures of 10, 100, 200, and 300 K. The interaction \mathcal{J} is measured in terms of the coupling constant C ; positive values corresponding to ferromagnetic coupling and negative to antiferromagnetic coupling. In the low-temperature regime (10 K) a distinct derivative discontinuity is seen at the antibonding band edge of 0.4 eV, which is, however, rapidly smoothed with increasing temperature.

the left-hand column the density plot indicates the *sign* of the interaction, i.e., whether at a particular separation and chemical potential the spins couple ferromagnetically ($\mathcal{J} > 0$) or antiferromagnetically ($\mathcal{J} < 0$). It is instructive to observe that the AFM region immediately above the antibonding band edge (indicated by the horizontal dashed line) continuously extends itself, as the temperature is increased, into energies below the antibonding band edge. It may also be observed how the separation of the interaction into two distinct regions $E > E_g$ and $E < E_g$ at 10 K gradually becomes less well defined as the temperature increases; indeed at 300 K the bands of FM/AFM regions have merged across $\mu = E_g$ such that the high-energy region transforms continuously into the low-energy region via series bifurcations of the FM/AFM bands. The right-hand column displays the same information but now as a density plot of the interaction strength scaled by R^2/μ ; evidently, as discussed above, the interaction is significantly stronger for $E > E_g$ than $E < E_g$ which is a consequence of the increased number of scattering channels in the two band region as compared to the single band region. To further illustrate this smoothing out of the $T = 0$ singularities we show in Fig. 8 the RKKY interaction plotted along the vertical line seen in Figs. 7(a)–7(d). As may be seen it is only at very low temperatures that a distinct singular behavior in the form of a derivative discontinuity may be observed.

V. SUMMARY AND CONCLUSIONS

We have investigated the effect of finite temperature on the RKKY interaction in single layer graphene and bilayer graphene. In different ways both systems display striking temperature anomalies. For the case of a single layer graphene the anomalous increase in the strength of the RKKY interaction

with increasing temperature is found in the undoped system. This effect is driven by the vanishing density of states at the Dirac point. The increase in temperature leads to an increase in the number of states available for scattering that counteracts the damping of the interaction due to the smearing of the Fermi surface. This physics is evidently very general, and a similar mechanism drives an anomalous increase in the conductivity with temperature in undoped graphene [20] which has been observed experimentally [19].

Interestingly, we find that the nature of the temperature dependence (normal, or anomalous) depends on the local coupling of the impurity to the graphene gas. For substitutional impurities the temperature dependence is always anomalous, but for plaquette impurities it depends on the particular coupling of the impurity to the six carbon atoms of the honeycomb cell. This result runs counter to what one might expect from the RKKY physics, in which the interaction is usually determined essentially by the *host material* and not the *specific impurity coupling*. It arises in graphene as the propagator of the host contains a factor that, due to the multivalley nature of the graphene spectrum, oscillates at the length scale of the graphene lattice constant. This renders the RKKY in graphene unusually sensitive to the details of the local coupling.

For the case of the bilayer the situation is different in that the $T = 0$ interaction of intercalated impurities residing between the two carbon layers shows an asymptotically discontinuous RKKY interaction. Below the antibonding band edge of $E_g = 0.4$ eV the interaction is oscillatory and is driven by a spanning vector of the low-energy-band Fermi surface [$k_F^+ = \sqrt{2}t_{\perp}/(\hbar v_F)$], but above the antibonding band edge this band “switches off” and the spanning vector is that of the high-energy bonding band (which evidently has $k_F^- = 0$ at the antibonding band edge). This entails a dramatic change in the magnetic interaction at the antibonding band edge. For chemical potentials close to the antibonding band edge, the effect of the smearing out of the Fermi surface at temperatures $T > 0$ is to “mix together” these distinct behaviors. In the case of chemical potentials that are below the antibonding band edge, but close to it, this results in a change *in the form of the RKKY interaction with temperature*: an oscillatory form of the interaction goes over to an antiferromagnetic form with increasing temperature. The temperature at which this crossover occurs is for $\mu = E_g$ approximately 10 K, and increases as the chemical potential is lowered from E_g . However, once the chemical potential is further than ≈ 30 meV from the antibonding band edge, the transition to an AFM behavior with temperature is lost as the Fermi smearing at finite temperatures can no longer access the states above the antibonding band edge.

ACKNOWLEDGMENTS

This work was supported by the European Science Foundation under the EUROCORES Program CRP Graphic-RF (DFG Grant No. PA 516/8-1), by the Special Priority Program “Graphene” (DFG Grant No. PA 516/9-1), and by the Collaborative Research Center SFB 953.

- [1] K. S. Novoselov, A. K. Geim, S. V. Morozov, D. Jiang, Y. Zhang, S. V. Dubonos, I. V. Grigorieva, and A. A. Firsov, *Science* **306**, 666 (2004).
- [2] K. S. Novoselov, A. K. Geim, S. V. Morozov, D. Jiang, M. I. Katsnelson, I. V. Grigorieva, S. V. Dubonos, and A. A. Firsov, *Nature (London)* **438**, 197 (2005).
- [3] A. H. Castro Neto, F. Guinea, N. M. R. Peres, K. S. Novoselov, and A. K. Geim, *Rev. Mod. Phys.* **81**, 109 (2009).
- [4] J. W. McClure, *Phys. Rev.* **104**, 666 (1956).
- [5] P. R. Wallace, *Phys. Rev.* **71**, 622 (1947).
- [6] S. Saremi, *Phys. Rev. B* **76**, 184430 (2007).
- [7] A. M. Black-Schaffer, *Phys. Rev. B* **81**, 205416 (2010).
- [8] M. Sherafati and S. Satpathy, *Phys. Rev. B* **83**, 165425 (2011).
- [9] M. Sherafati and S. Satpathy, *Phys. Rev. B* **84**, 125416 (2011).
- [10] A. M. Black-Schaffer, *Phys. Rev. B* **82**, 073409 (2010).
- [11] N. Klier, S. Shallcross, and O. Pankratov, *Phys. Rev. B* **90**, 245118 (2014).
- [12] J. H. Sun, F. M. Hu, H. K. Tang, W. Guo, and H. Q. Lin, *J. Appl. Phys.* **113**, 17B515 (2013).
- [13] J. M. Duffy, P. D. Gorman, S. R. Power, and M. S. Ferreira, *J. Phys.: Condens. Matter* **26**, 055007 (2014).
- [14] H. Lee, J. Kim, E. R. Mucciolo, G. Bouzerar, and S. Kettemann, *Phys. Rev. B* **85**, 075420 (2012).
- [15] H. Lee, E. R. Mucciolo, G. Bouzerar, and S. Kettemann, *Phys. Rev. B* **86**, 205427 (2012).
- [16] E. Kogan, *Phys. Rev. B* **84**, 115119 (2011).
- [17] L. Jiang, X. Lü, W. Gao, G. Yu, Z. Liu, and Y. Zheng, *J. Phys.: Condens. Matter* **24**, 206003 (2012).
- [18] F. Parhizgar, M. Sherafati, R. Asgari, and S. Satpathy, *Phys. Rev. B* **87**, 165429 (2013).
- [19] S. Tanabe, Y. Sekine, H. Kageshima, M. Nagase, and H. Hibino, *Phys. Rev. B* **84**, 115458 (2011).
- [20] N. Ray, S. Shallcross, S. Hensel, and O. Pankratov, *Phys. Rev. B* **86**, 125426 (2012).
- [21] J. Kleeman, K. Sugawara, T. Sato, and T. Takahashi, *Phys. Rev. B* **87**, 195401 (2013).
- [22] K. Sugawara, K. Kanetani, T. Sato, and T. Takahashi, *AIP Adv.* **1**, 022103 (2011).
- [23] C. Coletti, C. Riedl, D. S. Lee, B. Krauss, L. Patthey, K. von Klitzing, J. H. Smet, and U. Starke, *Phys. Rev. B* **81**, 235401 (2010).